THE JOURNAL OF PHYSICAL CHEMISTRY A

pubs.acs.org/JPCA Article

Anharmonic Frequencies of $(MO)_2$ and Related Hydrides for M = Mg, Al, Si, P, S, Ca, and Ti and Heuristics for Predicting Anharmonic Corrections of Inorganic Oxides

Brent R. Westbrook and Ryan C. Fortenberry*

Cite This: J. Phys. Chem. A 2020, 124, 3191−3204 Read Online

ACCESS | Metrics & More | Article Recommendations | Supporting Information

ABSTRACT: The low-frequency vibrational fundamentals of D_{2h} inorganic oxides are readily modeled by heuristic scaling factors at fractions of the computational cost compared to explicit anharmonic frequency computations. Oxygen and the other elements in the present study are abundant in geochemical environments and have the potential to aggregate into minerals in planet-forming regions or in the remnants of supernovae. Explicit quartic force field computations at the CCSD(T)-F12b/cc-pVTZ-F12 level of theory generate scaling factors that accurately predict the anharmonic frequencies with an average error of less than 1.0 cm^{-1} for both the metal−oxygen stretching frequencies and the torsion and antisymmetric stretching frequencies. Inclusion of hydrogen motions is less absolutely accurate but is similarly relatively predictive. The fundamental vibrational frequencies for the seven tetra-atomic inorganic oxides examined presently fall below 876 cm^{-1} and most of the hydrogenated species do as well. Additionally, ν_6 for the SiO dimer is shown to have an intensity of 562 km mol^{-1}, with each of the other molecules having one or more frequencies with intensities greater than 80 km mol^{-1}, again with most in the low-frequency infrared range. These intensities and the frequencies computed in the present study should assist in laboratory characterization and potential interstellar or circumstellar observation.

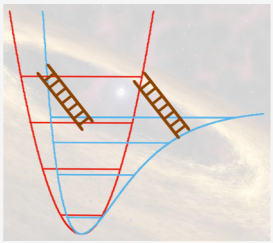

INTRODUCTION

Oxygen is the third most abundant element in the universe[1] and the most abundant element in the earth's crust,[2] making it a likely component in molecules for novel astrochemical searches. Previous work has shown that it behaves like a mortar holding inorganic elements together to form mineralogical compounds.[3,4] These mineral precursors may represent the early stages of planet formation or the remnants of planetary disintegration.[5−17] In either case, their detection aids in the understanding of planetary and stellar lifecycles. Many of these precursors are difficult to synthesize or to separate under laboratory conditions. Such species are perfectly suited to computational investigation.

Like oxygen, the other elements in the current study are abundant in space and contribute to the formation of interstellar dust grains[1] that could precede mineral formation. Of these compounds, $(MgO)_2$, $(AlO)_2$, $(SiO)_2$, $(PO)_2$, $(SO)_2$, $(CaO)_2$, and $(TiO)_2$, several of the monomeric versions have been previously detected in circumstellar or interstellar environments, including AlO,[18] SiO,[19,20] PO,[21] SO,[22] and TiO.[23] Additionally, closely related molecules such as SO_2,[24] SO^+,[25] and TiO_2[23] have also been detected in these regions, suggesting that there are more molecules composed of the same elements to be found in places such as VY Canis Majoris, Sagittarius B2, and Orion A, where these previous detections took place. In particular, the dimeric forms of the aforementioned monomers would likely occur wherever the monomers do, based on the strong dimerization energy of $(MgO)_2$.[26] However, they are more difficult to examine experimentally; their lack of a permanent dipole moment makes them invisible to rotational spectroscopy. Previous computational studies[27,28] show that the lowest-energy isomer of both $(AlO)_2$ and $(SiO)_2$ is the cyclic D_{2h} form, giving a basis for treating the other systems in the same way. Vibrational frequency data for the cyclic AlO[29] and SiO[30−32] dimers have been obtained previously in the laboratory. In the case of $(SiO)_2$, there is some inconsistency between the spectrum and the predicted features for the cyclic structure.[30] Consequently, a goal of the present work is to provide reliable spectroscopic data for these dimers in an effort to aid their detection in the interstellar medium, protoplanetary disks, or the outgassing of evolved stars.

The current state-of-the-art quantum chemical approach[33−43] for the production of accurate vibrational frequencies relies on a fourth-order Taylor series approximation to the internuclear potential. This method produces vibrational frequencies within 1.0 cm^{-1} of the gas-phase experiment in many cases. However, its high computational cost and use of symmetry-internal coordinates that can be difficult to determine for cyclic molecules limit the size and shape of the systems that can be analyzed. Nevertheless,

Received: February 24, 2020
Revised: March 20, 2020
Published: March 26, 2020

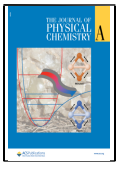

https://dx.doi.org/10.1021/acs.jpca.0c01609
J. Phys. Chem. A 2020, 124, 3191−3204

previous computational work[26] has elucidated the spectroscopic constants of the cyclic MgO dimer at this state-of-the-art level, providing a baseline comparison for the present work. A slightly less accurate but more computationally tractable method involving explicit correlation with only a triple-zeta basis set[44−47] is also often employed, which typically still gives vibrational frequencies within 7.0 cm^{-1} of the gas-phase experiment. The decreased computational requirements for this method generally make it worth the reduced accuracy, but greater improvements are highly desirable.

As a result of the computational demands required for these higher level procedures, the present study investigates the use of heuristic scaling factors to obtain usable anharmonic vibrational frequencies without the burden of computing them directly for inorganic oxides. Scaling factors have often been employed to bring computed harmonic frequencies inline with experimental results.[48−69] The generation of scaling factors based on a small series of molecules could aid in rapid generation of large amounts of accurate spectroscopic data that would allow for the characterization of experimental spectra in a way that would not be feasible using the aforementioned methods. Such data will be invaluable in analyzing the observations of new astronomical observatories such as the forthcoming *James Webb Space Telescope*.

COMPUTATIONAL DETAILS

Optimized geometries, harmonic frequencies, and dipole moments are computed using the Molpro 2015.1 software package[70] along with coupled cluster theory at the singles, doubles, and perturbative triples[71] level within the F12 explicitly correlated construction[72,73] (CCSD(T)-F12b). The cc-pVTZ-F12[44,74,75] basis set is used in all of these computations, with the exception of those involving calcium and titanium. For these, a default cc-pVTZ[76,77] basis is used, with a def2-TZVPP/jkfit[78] basis for the JK and RI portions of the energy computations. Furthermore, titanium requires an aug-cc-pVTZ[77] basis set for the DF portion, while calcium requires a def2-TZVPP/mp2fit[78] basis for the same, in a scheme previously demonstrated to give accurate results for other transition metals.[79] This scheme is abbreviated as F12-TZ in the following. Double-harmonic IR intensities utilize the Gaussian 16 program at the MP2/6-31+G* and B3LYP/cc-pVTZ levels of theory.[80−84] The first of these has been shown to agree semiquantitatively with more expensive levels of theory without commensurate computational requirements.[85,86]

The explicit anharmonic vibrational frequencies are computed using a quartic force field (QFF) approach at this F12-TZ level. The QFF method utilizes a fourth-order Taylor series expansion of the potential energy portion of the internuclear Watson Hamiltonian.[87] This involves optimization of the geometry to generate a reference configuration followed by 233 single-point energy computations for displacements of symmetry-internal coordinates of 0.005 Å and 0.005 radians in the case of the tetra-atomic D_{2h} molecules. Sulfur's deviation from the planar structure of the other molecules changes the symmetry from D_{2h} to C_{2v} and adds 120 more points for a total of 353. The additional atoms in the five- and six-atom hydride molecules increase these requirements to 1613 and 4565 points, respectively.

For the D_{2h} molecules, these symmetry-internal coordinates, with atomic labels defined in Figure 1, are as follows for the general atom M

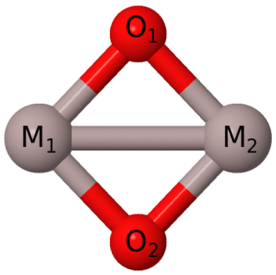

Figure 1. Visual depiction of the $(MO)_2$ molecule.

$$S_1(a_g) = \frac{1}{\sqrt{2}}[r(O_1 - O_2) + r(M_1 - M_2)] \quad (1)$$

$$S_2(a_g) = \frac{1}{\sqrt{2}}[r(O_1 - O_2) - r(M_1 - M_2)] \quad (2)$$

$$S_3(b_{1g}) = \frac{1}{2}[r(O_1 - M_1) - r(O_1 - M_2) - r(O_2 - M_1) + r(O_2 - M_2)] \quad (3)$$

$$S_4(b_{1u}) = \tau[O_2 - M_2 - M_1 - O_1] \quad (4)$$

$$S_5(b_{3u}) = \frac{1}{2}[r(O_1 - M_1) + r(O_1 - M_2) - r(O_2 - M_1) - r(O_2 - M_2)] \quad (5)$$

$$S_6(b_{2u}) = \frac{1}{2}[r(O_1 - M_1) - r(O_1 - M_2) + r(O_2 - M_1) - r(O_2 - M_2)] \quad (6)$$

Similarly, the symmetry-internal coordinates for $(SO)_2$ are given by interchanging the third and fourth coordinates

$$S_1(a_1) = \frac{1}{\sqrt{2}}[r(O_1 - O_2) + r(S_1 - S_2)] \quad (7)$$

$$S_2(a_1) = \frac{1}{\sqrt{2}}[r(O_1 - O_2) - r(S_1 - S_2)] \quad (8)$$

$$S_3(a_1) = \tau[O_2 - S_2 - S_1 - O_1] \quad (9)$$

$$S_4(a_2) = \frac{1}{2}[r(O_1 - S_1) - r(O_1 - S_2) - r(O_2 - S_1) + r(O_2 - S_2)] \quad (10)$$

$$S_5(b_1) = \frac{1}{2}[r(O_1 - S_1) + rO_1 - S_2) - r(O_2 - S_1) - r(O_2 - S_2)] \quad (11)$$

$$S_6(b_2) = \frac{1}{2}[r(O_1 - S_1) - r(O_1 - S_2) + r(O_2 - S_1) - r(O_2 - S_2)] \quad (12)$$

The analogous coordinates for the five-atom C_{2v} molecules, with labels being given in Figure 2, are

$$S_1(a_1) = r(M_1 - M_2) \quad (13)$$

$$S_2(a_1) = r(M_1 - H) \quad (14)$$

$$S_3(a_1) = \frac{1}{\sqrt{2}}[r(M_1 - O_1) + r(M_1 - O_2)] \quad (15)$$

https://dx.doi.org/10.1021/acs.jpca.0c01609
J. Phys. Chem. A 2020, 124, 3191−3204

$$S_4(a_1) = \frac{1}{\sqrt{2}}[\angle(H - M_1 - O_1) + \angle(H - M_1 - O_2)] \quad (16)$$

$$S_5(b_2) = \frac{1}{\sqrt{2}}[r(M_1 - O_1) - r(M_1 - O_2)] \quad (17)$$

$$S_6(b_2) = \frac{1}{\sqrt{2}}[\angle(M_2 - O_1 - M_1) + \angle(M_2 - O_2 - M_1)] \quad (18)$$

$$S_7(b_2) = \frac{1}{\sqrt{2}}[\angle(H - M_1 - O_1) - \angle(H - M_1 - O_2)] \quad (19)$$

$$S_8(b_1) = \mathrm{LIN}(M_2 - M_1 - H) \quad (20)$$

$$S_9(b_1) = \tau[O_1 - M_1 - H - O_2] \quad (21)$$

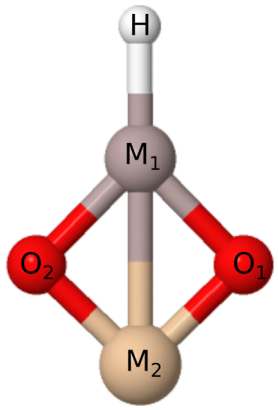

Figure 2. Visual depiction of the $HM_1M_2O_2$ molecule.

while those for the six-atom variants, with X = H/O and the labels shown in Figure 3, are

$$S_1(a_1) = r(M_1 - M_2) \quad (22)$$

$$S_2(a_1) = r(M_1 - H) \quad (23)$$

$$S_3(a_1) = \frac{1}{\sqrt{2}}[r(M_1 - O_1) + r(M_1 - O_2)] \quad (24)$$

$$S_4(a_1) = \frac{1}{\sqrt{2}}[\angle(H - M_1 - O_1) + \angle(H - M_1 - O_2)] \quad (25)$$

$$S_5(a_1) = r(M_2 - X) \quad (26)$$

$$S_6(b_2) = \frac{1}{\sqrt{2}}[r(M_1 - O_1) - r(M_1 - O_2)] \quad (27)$$

$$S_7(b_2) = \frac{1}{\sqrt{2}}[\angle(M_2 - O_1 - M_1) + \angle(M_2 - O_2 - M_1)] \quad (28)$$

$$S_8(b_2) = \frac{1}{\sqrt{2}}[\angle(H - M_1 - O_1) - \angle(H - M_1 - O_2)] \quad (29)$$

$$S_9(b_2) = \frac{1}{\sqrt{2}}[\angle(X - M_2 - O_1) - \angle(X - M_2 - O_2)] \quad (30)$$

$$S_{10}(b_1) = \mathrm{LIN}(M_2 - M_1 - H) \quad (31)$$

$$S_{11}(b_1) = \tau[O_1 - M_1 - H - O_2] \quad (32)$$

$$S_{12}(b_1) = \mathrm{LIN}(M_1 - M_2 - X) \quad (33)$$

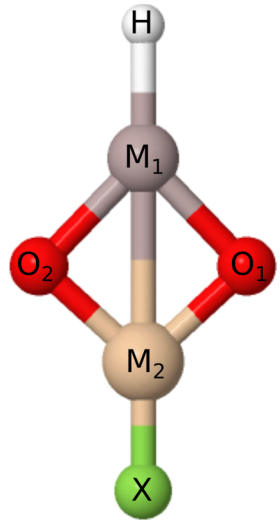

Figure 3. Visual depiction of the $HXM_1M_2O_2$ molecule.

where "LIN" in both of these cases corresponds to a linear bending mode, which happens to be out of plane in these systems.

In addition to the standard F12-TZ computations described above, the effects of core electron correlation are investigated for the third-row metal $(MO)_2$ molecules through the use of the cc-pCVTZ-F12[88] basis sets and core correlation ($1s^2$ for oxygen and $1s^22s^22p^6$ for the third-row atoms) turned on in the CCSD(T)-F12b computations. Magnesium additionally requires the use of a cc-pVTZ-F12/jkfit basis set for the DF portion of these energy computations.

Upon completion of the single-point computations, the QFF function is fit by a least-squares method with sums of squared residuals on the order of 10^{-16} a.u.^{2} or less in all cases. This fitted function gives the equilibrium geometry, and a refit produces the final force constants used to compute the anharmonic frequencies. The INTDER[89] program transforms the force constants into Cartesian coordinates for use in second-order rotational[90] and vibrational perturbation theory (VPT2)[91,92] within the SPECTRO[93] program. The force constants for each molecule are given in the Supporting Information. Fermi and Coriolis resonances are taken into account in these computations to increase the accuracy of the anharmonic values.[94,95] The resonances are shown in the Supporting Information. The frequency labels in Table 1 are ordered first by symmetry and then by the magnitude of the frequency. This ordering across molecules preserves the grouping of the modes into the M−O stretches and the torsion and antisymmetric bending modes, hereafter referred to as O bending modes. This convention is similarly maintained in Table 2. Differently, in Table 3, the modes are ordered relative to $HAlMgO_2$.

Anharmonic scaling factors for the harmonic frequencies are obtained using the harmonic and anharmonic frequencies generated by SPECTRO and are averaged in two groups for the tetra-atomic molecules. The first group includes the modes

https://dx.doi.org/10.1021/acs.jpca.0c01609
J. Phys. Chem. A 2020, 124, 3191−3204

Table 1. Explicit QFF Harmonic and Anharmonic Frequencies (in cm^{-1}) and Intensities (in km mol^{-1}) of the $(MO)_2$ Molecules, without Core Correlation

		Mg								
	symmetry	this work	CcCR[a]	diff	Al	Si	P	S[c]	Ca	Ti
ω_1	a_g	672.8	681.8	9.0	805.4	859.7	889.3	781.8	544.0	740.8
ω_2	a_g	449.0	450.3	1.3	524.3	560.5	622.9	519.2	295.8	425.7
ω_3	b_{1g}	573.1	580.7	7.6	647.7	579.8	710.6	658.4	428.3	441.0
ω_4	b_{1u}	285.3	286.9	1.6	302.0	238.5	437.2	297.1	207.4	190.0
ω_5	b_{2u}	664.1	673.6	9.5	774.9	783.8	754.8	755.3	508.2	706.6
ω_6	b_{3u}	607.4	615.0	7.6	679.9	827.1	647.3	674.0	643.0	715.2
$f(\omega_1)$[d]		0/0			0/0	0/0	0/0	6/6	0/0	0/0
$f(\omega_2)$[d]		0/0			0/0	0/0	0/0	2/1	0/0	0/0
$f(\omega_3)$[d]		0/0			0/0	0/0	0/0	0/0	0/0	0/0
$f(\omega_4)$[d]		140/146			51/40	2/1	35/28	12/8	181/150	236[b]/26
$f(\omega_5)$[d]		178/184			161/164	166/149	85/86	151/157	257/342	87/110
$f(\omega_6)$[d]		200/177			218/87	562/511	677/30	52/53	231/316	996/700
ZPVE		1619.8			1860.4	1918.6	2021.6	1832.0	1306.8	1604.2
ν_1	a_g	663.7	672.2	8.5	794.6	845.2	875.9	769.9	536.8	725.3
ν_2	a_g	446.1	450.3	4.2	520.8	557.3	617.1	510.6	293.9	422.3
ν_3	b_{1g}	562.3	569.4	7.1	634.9	565.8	692.6	643.1	420.0	435.7
ν_4	b_{1u}	283.4	284.4	1.0	300.4	240.2	432.6	287.2	207.0	193.2
ν_5	b_{2u}	653.0	661.8	8.8	762.6	772.1	742.8	741.3	501.2	697.4
ν_6	b_{3u}	597.3	605.0	7.7	667.2	813.1	633.4	664.0	627.7	696.8

[a]Previous results from ref 26. [b]Denotes imaginary frequency. [c]Actually C_{2v} symmetry. [d]Double-harmonic intensities at the MP2/6-31+G*/B3LYP/aug-cc-pVTZ levels of theory with the exception of Ca, which used cc-pVTZ for the B3LYP computations.

Table 2. Explicit QFF Harmonic and Anharmonic Frequencies (in cm^{-1}) of the Selected $(MO)_2$ Molecules, with Core Correlation via CCSD(T)-F12b/cc-pCVTZ

	symmetry	Mg	Al	Si	P	S[a]
ω_1	a_g	681.8	811.9	862.7	893.7	784.4
ω_2	a_g	453.6	527.0	562.0	625.6	521.6
ω_3	b_{1g}	581.2	653.6	580.5	714.5	660.8
ω_4	b_{1u}	287.3	304.1	238.9	441.3	298.3
ω_5	b_{2u}	674.5	783.4	786.8	757.2	757.5
ω_6	b_{3u}	614.7	674.4	829.7	643.9	675.8
ZPVE		1640.5	1869.3	1925.1	2029.0	1839.2
ν_1	a_g	673.0	801.0	848.5	881.3	772.2
ν_2	a_g	450.7	518.8	559.3	619.8	513.1
ν_3	b_{1g}	570.2	640.7	566.5	696.7	646.0
ν_4	b_{1u}	285.7	305.1	242.7	437.1	289.8
ν_5	b_{2u}	662.7	769.7	775.6	745.4	744.4
ν_6	b_{3u}	604.2	660.0	815.8	630.1	666.8
$\Delta(cC)_1$		−9.3	−6.4	−3.3	−6.9	−2.3
$\Delta(cC)_2$		−4.6	+2.0	−2.0	−2.7	−2.5
$\Delta(cC)_3$		−7.9	−5.8	−0.7	−4.1	−2.9
$\Delta(cC)_4$		−2.3	−4.7	−2.5	−4.5	−2.6
$\Delta(cC)_5$		−9.7	−7.1	−3.5	−2.6	−3.1
$\Delta(cC)_6$		−6.9	+7.2	−2.7	+3.3	−2.8
average	−3.5					
MAE	4.3					

[a]Actually C_{2v} symmetry.

with M−O stretches, while the second includes the remaining O bending modes. The percent anharmonicity is calculated for each fundamental frequency by taking the difference between the QFF anharmonic value and the harmonic value and dividing it by the harmonic. The scaling factor utilized is then the difference for each of these values from unity. The resulting scaling factors are averaged within the groups for all of the molecules and are multiplied with the harmonic frequencies, giving the scaled anharmonic frequencies. The difference between the scaled anharmonic frequencies and the explicit QFF anharmonic frequencies is then calculated as well. The simple average and mean absolute error (MAE), or the unsigned average, of these differences are given at the bottom of Table 4 for the tetra-atomic molecules. Scaling factors for the M−H stretching and bending modes and the coupled M−H bend/M−O stretch are generated by the same procedure applied to the five- and six-atom molecules. Modes are classified as shown in Table 5, and the average and MAE

https://dx.doi.org/10.1021/acs.jpca.0c01609
J. Phys. Chem. A 2020, 124, 3191−3204

Table 3. Explicit QFF Harmonic and Anharmonic Frequencies (in cm^{-1}) and Intensities (in km mol^{-1}) of the Hydride Molecules

	symmetry	$HAlMgO_2$	$HMgAlO_2$	$HSiAlO_2$	$HAlSiO_2$	$HAlSiO_3$	$HSiMgO_2H$
ω_1	a_1	1975.4	1606.3	2308.4	2032.6	2067.7	2328.3
ω_2	a_1	784.6	404.3	1049.0	844.2	800.1	1045.8
ω_3	a_1	671.8	887.8	526.0	804.2	844.7	539.4
ω_4	a_1	492.2	450.0	409.3	542.5	514.1	429.8
ω_5	a_1					402.1	218.5
ω_6	b_1	498.2	345.1	578.8	498.7	296.7	371.0
ω_7	b_1	268.9	245.4	213.6	248.3	548.8	803.4
ω_8	b_1					498.7	596.3
ω_9	b_2	776.4	1012.1	1137.5	820.0	1313.9	1624.0
ω_{10}	b_2	643.4	234.8	794.1	660.1	887.3	288.7
ω_{11}	b_2	558.3	363.9	194.0	549.4	690.7	1164.1
ω_{12}	b_2					167.0	341.5
$f(\omega_1)^a$		210	218	142	170	93	75
$f(\omega_2)^a$		113	125	69	4	300	95
$f(\omega_3)^a$		153	9	96	378	0	100
$f(\omega_4)^a$		6	0	177	7	186	56
$f(\omega_5)^a$						18	9
$f(\omega_6)^a$		153	316	52	161	14	206
$f(\omega_7)^a$		47	0	5	1	38	26
$f(\omega_8)^a$						4	58
$f(\omega_9)^a$		299	85	128	311	205	219
$f(\omega_{10})^a$		58	59	17	19	332	33
$f(\omega_{11})^a$		0	173	42	5	4	233
$f(\omega_{12})^a$						4	295
ZPVE		3313.6	2800.4	3578.7	3482.0	4464.7	4843.1
ν_1	a_1	1909.5	1549.5	2220.1	1967.1	1996.4	2245.8
ν_2	a_1	774.1	440.5	1033.1	832.4	784.9	1032.2
ν_3	a_1	661.4	876.4	519.9	791.1	833.1	534.5
ν_4	a_1	488.8	445.2	429.9	539.4	508.7	417.2
ν_5	a_1					381.9	219.8
ν_6	b_1	492.8	513.2	573.2	510.6	292.5	372.3
ν_7	b_1	267.7	321.9	213.2	248.8	494.7	792.7
ν_8	b_1					458.1	589.8
ν_9	b_2	764.6	996.9	1119.7	806.9	1259.8	1573.8
ν_{10}	b_2	634.9	205.6	786.4	648.3	867.8	279.9
ν_{11}	b_2	550.6	297.2	178.9	538.6	676.6	1148.5
ν_{12}	b_2					173.5	343.6

[a]Double-harmonic intensities at the MP2/6-31+G* level of theory.

differences between the QFF and scaled results are reported in Table 6. The generated scaling factors are also applied to molecules from the recent literature[3,41,96] and their performance is compared to the reported anharmonic corrections, as shown in Table 7.

RESULTS AND DISCUSSION

Explicit Anharmonic Frequencies. The anharmonicities for these molecules are rather small, with all of them falling below 20 cm^{-1}. This is a testament to the rigidity of the M−O bonds, which can be judged most directly by the magnitudes of the force constants in the O−O and M−M coordinates. The symmetric and antisymmetric pairings of these occur in the first two coordinates, so F_{11} and F_{22} give good estimates of their strength. As shown in the Supporting Information, the greatest of these force constants occurs in the F_{11} of $(PO)_2$ at 4.69 mdyn/Å^2, and the rest of the associated constants for the other tetra-atomic molecules are greater than 1.8 mdyn/Å^2. This makes them roughly comparable to other third-row atom single bonds in terms of their strength.[41,86]

The present F12-TZ QFF values for $(SiO)_2$ of 772.1 and 813.1 cm^{-1} for ν_5 and ν_6, respectively, from Table 1, compare quite favorably with those determined by Anderson and Ogden[31] of 766.3 and 804.7 cm^{-1}. This is especially true because these experimental data are obtained in nitrogen and argon matrices. Such spectroscopic techniques likely red-shift the observed spectra versus gas-phase frequencies.[31] Similarly, the herein reported values are also comparable to those obtained by Khanna, et al.[30] of 804.4, 765.5, and 252 cm^{-1} in an N_2 matrix, with the lowest of these coming close to the F12-TZ QFF value of 240.2 cm^{-1} for ν_4. A more recent Ar matrix study[32] yields values of 803.2 and 768.2 cm^{-1}, which again compare favorably with the values reported here. For $(AlO)_2$, the present values for ν_1, ν_6, and ν_2 of 794.6, 667.2, and 520.8 cm^{-1}, respectively, are nearly identical to cryogenic velocity-map imaging experimental data obtained by DeVine et al. at 794, 663, and 523 cm^{-1}.[98]

Additionally, the present F12-TZ value of 501.2 cm^{-1} for ν_5 of $(CaO)_2$ compares well with the nitrogen matrix results of 497.0 cm^{-1} obtained by Andrews et al.[99] This agreement is

https://dx.doi.org/10.1021/acs.jpca.0c01609
J. Phys. Chem. A 2020, 124, 3191−3204

Table 4. Anharmonic Frequency Corrections and Scaling Factors for $(MO)_2$ Molecules

M	fundamental	anharmonic correction	percent anharm	scaled anharm	QFF-scaled diff.	T_1 diag.
Mg	ν_1	9.1	1.353	661.0	−1.9	0.022
	ν_3	10.8	1.884	563.0	0.7	
	ν_5	11.1	1.671	652.4	−0.6	
	ν_6	10.1	1.663	596.7	−0.6	
	ν_2	2.9	0.646	445.7	−0.4	
	ν_4	1.9	0.666	283.2	−0.2	
Al	ν_1	10.8	1.341	791.2	−3.4	0.023
	ν_3	12.8	1.976	636.3	1.4	
	ν_5	12.3	1.587	761.3	−1.3	
	ν_6	12.7	1.868	667.9	0.7	
	ν_2	3.6	0.687	520.4	−0.4	
	ν_4	1.6	0.530	299.8	−0.6	
Si	ν_1	14.5	1.687	844.6	−0.6	0.016
	ν_3	14.0	2.415	569.6	3.8	
	ν_5	11.7	1.493	770.0	−2.1	
	ν_6	14.0	1.693	812.6	−0.5	
	ν_2	3.2	0.571	556.4	−0.2	
	ν_4	−1.7	−0.713	236.7	−3.5	
P	ν_1	13.4	1.507	873.7	−0.7	0.015
	ν_3	18.0	2.533	698.1	5.5	
	ν_5	12.0	1.590	741.5	−1.3	
	ν_6	13.9	2.147	635.9	2.5	
	ν_2	5.8	0.931	618.3	1.2	
	ν_4	4.6	1.052	434.0	1.4	
S	ν_1	11.9	1.522	768.1	−1.8	0.017
	ν_3	15.3	2.324	646.8	3.7	
	ν_5	14.0	1.854	742.0	0.7	
	ν_6	10.0	1.484	662.2	−1.8	
	ν_2	8.6	1.656	515.4	4.4	
	ν_4	9.9	3.332	294.9	7.7	
Ca	ν_1	7.2	1.324	534.4	−1.6	0.024
	ν_3	8.3	1.938	420.8	0.8	
	ν_5	7.0	1.377	499.3	−1.9	
	ν_6	15.3	2.379	631.7	4.0	
	ν_2	1.9	0.642	293.6	−0.3	
	ν_4	0.4	0.193	205.9	−1.1	
Ti	ν_1	15.5	2.092	727.8	−4.8	0.060
	ν_3	5.3	1.202	433.2	−2.5	
	ν_5	9.2	1.302	694.2	−3.2	
	ν_6	18.4	2.573	702.6	5.8	
	ν_2	3.4	0.799	422.6	4.5	
	ν_4	−3.2	−1.684	188.6	−4.6	
	M−O stretch avg corr				0.0	
	O stretch avg corr				0.6	
	M−O stretch MAE corr				2.2	
	O stretch MAE corr				2.2	

preserved in isotopic substitution computations, where one and then both of the oxygen atoms are replaced with ^{18}O. Andrews et al. obtain values of 489.4 and 481.2 cm^{-1} for this mono- and disubstitution, respectively, while the F12-TZ methodology gives results of 488.5 and 481.1 cm^{-1}.[99] However, the other frequency assigned to $(CaO)_2$ by Andrews et al. of 559.5 cm^{-1} does not agree well with any of the presently computed values. This value is more than 20 cm^{-1} higher than the present value of 536.8 cm^{-1} for ν_1, and the double-harmonic intensity computations suggest that this frequency would be invisible to the experiment, regardless. This leaves ν_6 as the closest possible counterpart in the present study, but its value of 627.7 cm^{-1} is well beyond the expected error for the F12-TZ methodology. In contrast, one of the frequencies assigned by Andrews et al. to CaO_3 at 633.9 cm^{-1} does agree well with our value for ν_6. Comparing the ^{18}O results strengthens this similarity, with the computed value of 602.2 cm^{-1} coming even closer to the experimental value of 599.7 cm^{-1}.[99] Hence, the present study implies that this band previously assigned to CaO_3 likely correlates to $(CaO)_2$.

As alluded to above, the computed frequencies that are detectable are those where the dipole moment shifts with the motions of the atoms. This narrows the observable frequencies for each of the tetra-atomic molecules (save for the SO dimer) to those with b_{2u}, b_{3u}, and b_{1u} symmetries. Although ν_4 has the lowest nonzero intensity for each of the molecules, as shown in

https://dx.doi.org/10.1021/acs.jpca.0c01609
J. Phys. Chem. A 2020, 124, 3191−3204

Table 5. Anharmonic Frequency Corrections and Scaling Factors for the Hydride Molecules

molecule	fundamental	anharmonic correction	percent anharm.	scaled anharm.	QFF-scaled diff	T_1 diag.
$HAlMgO_2$	ν_1[a]	65.8	3.336	1907.6	1.9	0.018
	ν_2[b]	10.5	1.338	770.8	3.3	
	ν_3[b]	10.3	1.548	660.0	1.4	
	ν_4[e]	3.4	0.691	488.6	0.2	
	ν_6[d]	5.4	1.084	492.4	0.4	
	ν_7[e]	1.2	0.446	266.9	0.8	
	ν_9[b]	11.7	1.520	762.8	1.8	
	ν_{10}[c]	8.5	1.321	628.0	7.1	
	ν_{11}[c]	7.7	1.379	545.0	5.1	
$HMgAlO_2$	ν_1[a]	56.8	3.536	1551.1	−1.6	0.022
	ν_2[b]	−36.2	−8.954	397.2	0.1	
	ν_3[b]	11.4	1.284	872.2	3.1	
	ν_4[e]	4.8	1.067	446.7	−1.5	
	ν_6[d]	−168.1	−48.711	341.1	172.1	
	ν_7[e]	−76.5	−31.174	243.6	78.3	
	ν_9[b]	15.2	1.502	994.3	2.8	
	ν_{10}[c]	29.2	12.436	229.2	−23.6	
	ν_{11}[c]	66.7	18.329	355.2	−57.8	
$HSiAlO_2$	ν_1[a]	88.3	3.825	2229.1	−4.5	0.018
	ν_2[b]	15.9	1.516	1030.6	2.5	
	ν_3[b]	6.1	1.160	516.8	3.1	
	ν_4[e]	−20.6	−5.033	406.3	−3.3	
	ν_6[d]	5.6	0.968	572.0	1.2	
	ν_7[e]	0.5	0.187	212.0	1.2	
	ν_9[b]	17.8	1.565	1117.5	4.7	
	ν_{10}[c]	7.7	0.970	775.1	10.3	
	ν_{11}[c]	15.1	7.784	189.4	−10.5	
$HAlSiO_2$	ν_1[a]	65.5	3.222	1962.8	4.3	0.016
	ν_2[b]	11.8	1.398	829.4	3.0	
	ν_3[b]	13.1	1.629	790.1	1.0	
	ν_4[e]	3.1	0.571	538.5	0.1	
	ν_6[d]	−11.9	−2.386	492.9	17.7	
	ν_7[e]	−0.5	−0.201	246.5	2.3	
	ν_9[b]	13.1	1.598	805.6	1.3	
	ν_{10}[c]	11.7	1.788	644.3	4.0	
	ν_{11}[c]	10.8	1.966	536.3	2.3	
$HAlSiO_3$	ν_1[a]	71.4	3.448	1996.7	−0.3	0.050
	ν_2[b]	15.2	1.900	786.0	0.3	
	ν_3[b]	11.6	1.373	829.9	3.5	
	ν_4[e]	5.4	1.050	510.3	−1.6	
	ν_5[e]	20.2	5.024	399.1	−16.1	
	ν_6[d]	4.2	1.416	293.2	−0.7	
	ν_7[e]	54.1	9.858	544.7	−37.0	
	ν_8[d]	40.6	8.141	492.9	−34.8	
	ν_9[b]	54.2	4.118	1290.8	−31.0	
	ν_{10}[c]	19.5	2.198	866.1	1.7	
	ν_{11}[c]	14.1	2.041	674.2	3.2	
	ν_{12}[e]	−6.5	−3.892	165.8	7.7	
$HSiMgO_2H$	ν_1[a]	82.5	3.543	2248.3	382.9	0.022
	ν_2[b]	13.6	1.300	1027.4	4.8	
	ν_3[b]	4.9	0.908	529.9	−7.7	
	ν_4[e]	12.6	2.932	426.6	−10.1	
	ν_5[d]	−1.4	−0.595	215.9	3.9	
	ν_6[d]	−1.3	−0.350	366.7	5.6	
	ν_7[e]	10.7	1.332	797.5	−4.4	
	ν_8[d]	6.5	1.090	589.3	0.5	
	ν_9[b]	50.2	3.091	1595.5	−21.7	
	ν_{10}[c]	8.8	3.048	281.8	−1.9	
	ν_{11}[c]	15.6	1.340	1136.3	12.2	
	ν_{12}[b]	−2.1	−0.615	335.5	8.1	

https://dx.doi.org/10.1021/acs.jpca.0c01609
J. Phys. Chem. A 2020, 124, 3191−3204

Table 5. continued

[a]MH stretch. [b]MO stretch. [c]MH bend and MO stretch. [d]MH bend. [e]MO bend.

Table 6. Results of Applying Scaling Factors to the Hydride Molecules

	scaling factor	QFF-scaled avg. diff.	QFF-scaled MAE diff.
M−O stretch	0.98242	−0.8	5.5
O bend	0.99261	1.2	11.8
M−H stretch	0.96565	0.0[a]	2.5[b]
H bend	0.98829	−0.8[c]	8.1[d]
M−O stretch + H bend	0.97610	−4.0	11.6

[a]Including the large contribution from $HSiMgO_2H$ increases this to 63.8. [b]Including the large contribution from $HSiMgO_2H$ increases this to 65.9. [c]Including the large contribution from $HMgAlO_2$ increases this to 18.4. [d]Including the large contribution from $HMgAlO_2$ increases this to 26.3.

Table 7. Scaling Factors Applied to Literature Molecules

molecule	fundamental	previous harmonic	previous anharmonic	total scaled anharm.	QFF-total scaled diff.
$MgSiO_3$[a]	ν_1	1278.6	1261.8	1256.1	−5.7
	ν_2	872.7	858.8	857.3	−1.4
	ν_3	824.7	812.0	810.2	−1.8
	ν_4	710.1	700.3	697.6	−2.7
	ν_5	618.1	608.2	607.2	−1.0
	ν_6	483.2	479.9	479.6	0.8
	ν_7	431.6	428.7	428.4	−0.3
	ν_8	310.0	308.2	307.7	−0.5
	ν_9	165.4	164.7	164.2	−0.5
	M−O stretch avg				−2.5
	O bend avg				−0.1
	M−O stretch MAE				2.5
	O bend MAE				0.5
$HOSi^+$[b]	ν_3	1121.5	1101.2	1101.8	0.6
$HSiO^+$[b]	ν_1	2244.4	2158.9	2167.3	−8.4
	ν_3	1262.3	1246.3	1240.1	−6.2
HPO[b]	ν_1	2165.6	2055.7	2091.2	−35.5
	ν_3	1211.8	1197.8	1190.5	−7.3
HSO^+[b]	ν_1	3517.9	3323.2	3397.1	−73.9
	ν_3	1238.3	1219.6	1216.5	−3.1
HOS^+[b]	ν_3	1045.6	1029.3	1027.2	−2.1
SNO^-[c]	ν_2	497.6	490.9	488.9	−2.0
OSN^-[c]	ν_3	1015.0	999.4	997.2	−2.2
	M−O stretch avg				−3.2
	M−O stretch MAE				3.4
	M−H stretch avg				−39.3
	M−H stretch MAE				39.3
	overall M−O stretch avg				−2.9
	overall M−O stretch MAE				3.0
	overall M−H stretch avg				−39.3
	overall M−H stretch MAE				39.3

[a]CCSD(T)-F12/cc-pVTZ-F12 QFF from ref 3. [b]CcC QFF from ref 41. [c]CcCR QFF from ref 97.

Table 1, most are at or above the intensity for the antisymmetric stretch of water at 70 km mol^{-1}. Between ν_5 and ν_6, ν_6 is typically the most intense, with that of $(TiO)_2$ being the brightest, followed by $(SiO)_2$ and $(PO)_2$. The same mode of $(PO)_2$ demonstrates significant disagreement between the two intensity computations, but the MP2 results are likely more trustworthy based on previous work.[85]

With this in mind, only the MP2 intensities are reported for the hydride molecules. Each of these molecules contains at least four modes with intensities greater than the aforementioned antisymmetric stretch of water. Because of the greater variation in electronic arrangement between these molecules, generalization about which mode is the most intense is more difficult. In every case, the first a_1 mode and the first b_2 mode, corresponding to ν_1 and ν_9, respectively, have intensities of greater than 70 km mol^{-1}. Directly comparable experimental data are not available to gauge the performance of the F12-TZ QFF methodology. However, the presence of a permanent dipole moment in each of these molecules offers a chance to first observe them through rotational spectroscopy that is not possible for the tetra-atomic structures. This would allow for initial characterization of these molecules before vibrational studies that can be performed with much higher confidence. Such necessary rotational data are also provided in Table 9. A_0, B_0, and C_0 therein correspond to the rotational constants in the ground vibrational state, while A_e, B_e, and C_e are those for the equilibrium geometry. Similarly, in Table 8, A_n, B_n, and C_n are the rotational constants for the first vibrationally excited state in the mode n.

The T_1 diagnostics for all but two molecules fall within the acceptable range. The T_1 diagnostic is often used as a measure of a system's multireference character, with values of roughly 0.02 and lower corresponding to a reasonably low multireference character.[100] As such, the methods used herein seem appropriate for the treatment of the molecules in the two series, but $(TiO)_2$ and $HAlSiO_3$ likely have some characteristics that cannot be as well described because of their respective T_1 diagnostics of 0.060 and 0.050, as given in Tables 4 and 5. This casts some doubt on the accuracy of the frequencies obtained for these structures, but their contributions to the scaling factors should not affect any of the major results.

Another trend is the increasingly prolate nature of the tetra-atomic molecules as the molecular mass increases. $(MgO)_2$, with the second-longest O−O bond length, is oblate, as shown in Figure 4, because its A and B rotational constants (Table 8) are close in magnitude. The molecules take on more of a prolate structure when moving across the periodic table to more massive M. The size of the B rotational constant also decreases relative to the A constant, putting it closer to the C constant. This trend continues on the next row for calcium and titanium. The titanium oxide dimer is the most prolate of the tetra-atomics based on the similarity of its B and C rotational constants and the proportionately larger A constant, as shown in Table 8. This trend repeats with the five- and six-atom molecules, with those containing the heavy silicon atom having A constants that are relatively greater than the B and C constants, as shown in Table 9 and Figure 5.

Scaling Factors. Applying the grouped scaling factors generated from all seven tetra-atomic molecules (0.98242 and 0.99261) in Table 4 yields an average correction of 0.0 cm^{-1}, a fortuitous coincidence here, for the M−O stretches and only 0.6 cm^{-1} for the O bends. Regardless, these values suggest that there is little difference between the explicitly computed QFF

https://dx.doi.org/10.1021/acs.jpca.0c01609
J. Phys. Chem. A 2020, 124, 3191−3204

Table 8. Bond Lengths and Rotational Constants of the $(MO)_2$ Molecules

	units	Mg	Al	Si	P	S[a]	Ca	Ti
R_0(M−O)	Å	1.87417	1.75161	1.69635	1.66137	1.70175	2.14386	1.83246
R_0(O−O)	Å	2.86784	2.53910	2.34691	2.22205	2.29398	3.00359	2.49236
A_0	MHz	7697.2	9818.3	11,491.0	12,823.2	11,125.8	7017.1	10,185.9
B_0	MHz	7247.6	6440.5	6027.0	5354.0	5371.7	2704.3	2922.6
C_0	MHz	3727.9	3884.9	3949.7	3773.0	3806.1	1950.3	2269.5
A_4	MHz	7681.6	9792.6	11,454.0	12,753.4	11,116.7	6997.6	10,144.0
B_4	MHz	7224.3	6430.4	6025.3	5335.5	5355.6	2703.9	2926.7
C_4	MHz	3731.3	3889.7	3956.9	3774.0	3794.7	1952.6	2274.7
A_5	MHz	7697.6	9828.6	11,509.9	12,874.4	11,090.2	7032.6	10,202.3
B_5	MHz	7219.4	6417.9	6007.0	5338.0	5358.5	2698.1	2915.2
C_5	MHz	3715.0	3873.4	3938.8	3763.1	3797.1	1946.3	2264.3
A_6	MHz	7713.2	9776.8	11,449.9	12,773.8	11,154.2	6979.3	10,143.1
B_6	MHz	7247.3	6446.2	6024.7	5357.7	5366.8	2704.4	2921.6
C_6	MHz	3725.4	3874.5	3939.6	3761.2	3794.8	1946.0	2265.2
Δ_J	kHz	3.625	2.103	1.590	1.031	1.593	0.478	0.362
Δ_K	kHz	8.636	8.211	8.571	11.177	13.186	9.269	9.793
Δ_{JK}	kHz	−5.557	−1.429	2.062	1.685	−1.018	−0.704	1.317
δ_J	kHz	1.547	0.813	0.561	0.310	0.389	0.159	0.095
δ_K	kHz	1.137	2.425	3.891	2.746	2.542	1.127	1.887
Φ_J	mHz	6.020	1.987	1.254	0.493	1.278	0.330	0.090
Φ_K	mHz	41.914	44.036	57.504	40.190	52.432	43.653	35.367
Φ_{JK}	mHz	−23.097	−6.863	−7.661	−1.889	−3.354	−1.044	−2.244
Φ_{KJ}	mHz	−10.722	−21.367	−27.727	−17.401	−23.118	−11.662	−9.304
ϕ_J	mHz	3.008	0.990	0.620	0.241	0.569	0.158	0.044
ϕ_{JK}	mHz	−6.065	−1.005	−1.475	0.529	1.186	0.475	−0.793
ϕ_K	mHz	11.259	18.157	34.670	27.991	30.757	17.776	26.450
dipole	D	0.0	0.0	0.0	0.0	0.5	0.0	0.0

[a]Sulfur has an additional dihedral angle of 141.06260704° (O−S−S−O).

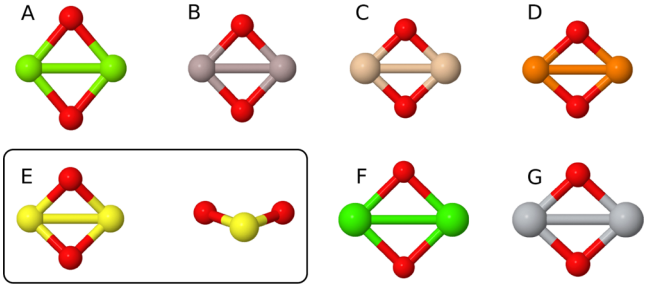

Figure 4. Optimized geometries of the D_{2h} $(MO)_2$ molecules, where M is (A) Mg, (B) Al, (C) Si, (D) P, (E) S [C_{2v}], (F) Ca, and (G) Ti.

anharmonic frequencies and the scaled frequencies for the oxygen stretching frequencies in those relatively low-frequency motions of these small molecules. Similarly, the difference for the oxygen bending frequencies is an order of magnitude smaller than the expected error for the explicit computation,[46,47] indicating that there is effectively minimal difference for these frequencies as well.

The performance of the other scaling factors is somewhat less impressive when applied to the five- and six-atom molecules. The MAE difference between the explicit QFF and scaled values is 5.5 cm^{-1} for the M−O stretching modes of these molecules, which is greater than the 0.0 cm^{-1} for the tetra-atomics but still within the estimated error of the QFF

Table 9. Geometrical Parameters and Rotational Constants for the Hydride Molecules

	units	$HAlMgO_2$	$HMgAlO_2$	$HSiAlO_2$	$HAlSiO_2$	$HAlSiO_3$	$HSiMgO_2H$
$R_0(M_1-H)$	Å	1.57283	1.70754	1.46868	1.56067	1.55272	1.46602
$R_0(M_1-O)$	Å	1.73165	2.10451	1.56249	1.73997	1.74950	1.55893
$R_0(M_2-O)$	Å	1.86560	1.64651	2.01284	1.68388	1.64742	2.07348
$R_0(M_1-M_2)$	Å	2.41690	2.46418	2.50455	2.41794	2.38620	2.51379
$\angle(H-M_1-O)$	deg	129.814	138.685	126.565	135.860	136.344	124.596
$R_0(M_2-N)$	Å					1.51021	1.70323
$\angle(N-M_2-O)$	deg					132.853	141.764
A_0	MHz	8896.1	8155.2	9986.6	10,725.2	10,794.5	9553.3
B_0	MHz	6175.4	5669.9	5305.4	5707.2	2731.4	5046.5
C_0	MHz	3641.4	3338.8	3458.7	3721.9	2179.0	3298.3
A_e	MHz	8936.5	8193.3	10,035.9	10,773.6	10,845.9	9593.4
B_e	MHz	6201.2	5702.4	5339.9	5729.3	2740.1	5075.2
C_e	MHz	3660.8	3362.2	3485.4	3740.2	2187.6	3319.3
dipole moment	D	6.4	5.7	3.6	2.1	6.3	3.4

https://dx.doi.org/10.1021/acs.jpca.0c01609
J. Phys. Chem. A 2020, 124, 3191−3204

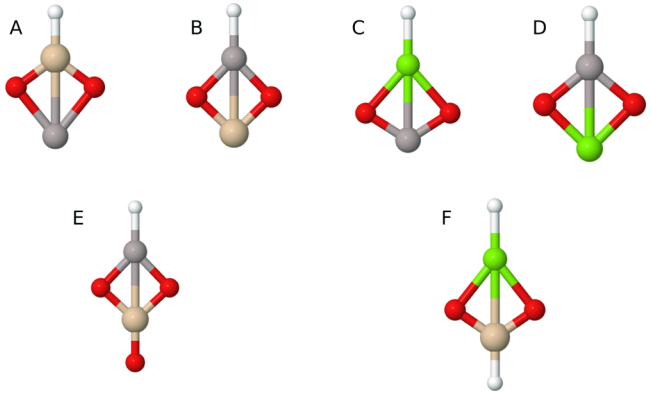

Figure 5. Optimized geometries of the C_{2v} $H(X)M_1M_2O_2$ molecules, where the molecular formulas are (A) $HSiAlO_2$, (B) $HAlSiO_2$, (C) $HMgAlO_2$, (D) $HAlMgO_2$, (E) $HAlSiO_3$, and (F) $HMgSiO_2H$.

methodology of 5−7 cm^{-1}. In contrast, the MAE difference for the O bending motion falls outside this range at 11.8 cm^{-1}. Similarly, the MAE for the M−H stretch (2.5 cm^{-1}) but not the H bend (8.1 cm^{-1}) is within these bounds, while that for the modes that combine M−H bending and M−O stretching motions is also beyond the expected range at 11.6 cm^{-1}. Somewhat unsurprisingly, including the sign of the differences decreases the apparent deviation thanks to a cancellation of positive and negative errors.

Despite the decreased performance on these molecules, the overall agreement between the explicitly computed and scaled anharmonic frequencies is still quite sufficient for future studies where large potential energy surfaces or even QFFs are not possible. The five- and six-atom molecules studied herein also demonstrate strong coupling between the different vibrational motions, making it difficult to determine which scaling factor to use. When these motions are more readily distinguishable, the scaling factors will likely perform better, as they do for the tetra-atomics. The data presented in the body of Table 6 also leave out only the most egregious outliers for the QFF-scaled difference, which all contain magnesium in an extended valence construction. These additional interactions are likely unstable for hydrides. Regardless, a more liberal assignment of outliers would improve the average and MAE results substantially but not to the point where this is absolutely essential for meaningful predictions of the fundamental frequencies.

The anharmonic scaling factors derived here for tetra-atomic inorganic oxides perform well not only on the molecules from which they were calculated but also on similar molecules from the recent literature, implying a more general behavior. As shown in Table 7, the average difference between the reported explicit anharmonic frequencies and the scaled frequencies for $MgSiO_3$ is −2.5 and −0.1 cm^{-1} again for the M−O stretches and the O bending frequencies, respectively. The MAEs for the same groups are 2.5 and 0.5 cm^{-1}. For the triatomic molecules mentioned in Table 7, the average M−O stretch difference is −3.2 cm^{-1} and the MAE is 3.4 cm^{-1}. Combining these with the $MgSiO_3$ M−O stretching frequency data gives an overall average correction of −2.9 cm^{-1} and a very similar MAE of 3.0 cm^{-1}. Although these corrections are larger than those obtained on the tetra-atomic training set, they are still less than half the size of the error inherent in the QFF method used herein.[46,47] This suggests that the relative accuracy of the scaled anharmonic corrections is comparable to the explicit QFF results, again providing promise for scaling factors applied to much larger systems.

The M−H stretching scaling factor derived from the five- and six-atom molecules does not perform quite as well on these literature molecules, as demonstrated by the MAE of 39.3 cm^{-1}, as shown in Table 7. Although this MAE is quite a bit larger than that observed for the M−O stretching modes, the absolute frequencies of the M−H stretches are much higher. In particular, the H−S stretch of HSO^+ has a previously reported fundamental frequency of 3323.2 cm^{-1}. Taking its relatively massive QFF-scaled difference of −73.9 cm^{-1} relative to this yields only a 2% error, which is comparable to the roughly 0.1% error for the best-behaved of the other scaled harmonic values in ν_7 of $MgSiO_3$. This is still over an order of magnitude difference, but the extent of the error for the M−H stretches is still much smaller than the anharmonic correction itself; therefore, the scaled values offer some, even if not ideal, improvement on the harmonic values, regardless.

On a related note, it would be ideal to have a uniform scaling factor to apply to all of the harmonic frequencies produced by a given methodology. However, the range of magnitudes of the frequencies in question is so large that an average over all of the modes would treat those at the extreme high and low ends quite poorly. Losing some convenience in application by requiring the classification of particular modes leads to substantial gains in accuracy that should be worth the trade-off for most applications.

In the case of the tetra-atomic D_{2h} molecules studied here, 233 single-point energy computations are needed to obtain the explicit anharmonic frequencies, while only 21 are present to obtain harmonic frequencies by the same method. In terms of time, the 233 points for $(MgO)_2$ require a total of 40,787 s (11.3 h) on our local system, while the harmonic frequencies require only 3676 s (1.0 h). By either measure, this reflects a difference of an order of magnitude in computational cost reduction, and the marginal accuracy gains do not require using the more rigorous method for most applications such as comparison to high-resolution experimental data. Furthermore, the time increase compounds geometrically for larger systems, making the eventual extension of the QFF methodology to extended molecules and clusters virtually unthinkable.

Core Correlation. Core electron correlation has been shown to be necessary to include in constructing QFFs that approach a spectroscopic accuracy of 1.0 cm^{-1}.[33,34] However, such accuracies are only meaningful for inclusion at the triple-zeta basis level which is where the F12-TZ approach is already settled. Hence, any inclusion of core correlation for the F12-TZ level will be performed within the level of theory itself and cannot be in a time-saving composite approach.

CCSD(T)-F12b/cc-pCVTZ-F12 QFF anharmonic vibrational frequencies in Table 2 agree very well with the previously reported CcCR data for $(MgO)_2$ but are farther from the available experimental results than the F12-TZ frequencies in all cases but one. The $(SiO)_2$ ν_4 of 242.7 cm^{-1} from the core-correlated QFF comes slightly closer to the experimental data than its F12-TZ counterpart. This one instance of improved agreement appears to result from the fact that the core-correlated frequencies are greater than the non-core-correlated frequencies in every other case, and the experimental result is actually greater than the F12-TZ result for this one result. Disregarding this slightly better agreement with the experimental data, the MAE difference between the core and noncore computations is only 4.3 cm^{-1}, which is

https://dx.doi.org/10.1021/acs.jpca.0c01609
J. Phys. Chem. A 2020, 124, 3191−3204

within the expected error for the F12-TZ QFF methodology. Although such an accuracy is needed in some cases, other systems may not require or be possible to treat with such quantum chemical rigor.

Even if this difference brought the results closer to those of the experiment, the greater computational demand of the core-correlating computations would likely not justify this slight increase in accuracy, at least for future application to larger inorganic oxide molecules. The energy points for the QFFs for $(MgO)_2$, $(AlO)_2$, $(SiO)_2$, $(PO)_2$, and $(SO)_2$ require a total of 454,695 s (5.3 days) without core correlation, while the corresponding energy computations with core correlation on the same computing system require 5,949,850 s (68.9 days), a 13-fold increase. Although running these jobs massively in parallel, as they are in this work, will decrease the wall time required, this measure vividly demonstrates the substantial difference in computational requirements for the two methods.

Similarly, comparison to the CcCR data for $(MgO)_2$ suggests that the inclusion of relativistic effects and a complete basis set extrapolation offer only minor improvements over the reported F12-TZ results with yet another increase in required computational time. Although the differences between the core-correlated and the non-core-correlated computations on this molecule are on the order of 5−10 cm^{-1}, the disparities between the core-correlated and CcCR data are all less than or equal to 1.3 cm^{-1}, with most of these less than 1.0 cm^{-1}. Hence, if more accurate data are required and the size of the system affords it, the addition of core-correlation should be the most impactful improvement. However, the inclusion of these effects seems unnecessary for the treatment of the current systems, and such an increase in computational time would be wholly intractable when extending this methodology to larger covalent networks. This could further reduce the sizes of molecules for which F12-TZ computations are possible and would do so for little-to-no-gain based on the present results.

CONCLUSIONS

Anharmonic scaling factors developed in this work are largely predictive of fundamental vibrational frequencies. These values allow for the computation of anharmonic frequencies at relatively high levels of theory for systems well beyond the size benchmarked here, where explicit anharmonic methods are not feasible. The anharmonic scaling factors developed in this study on a training set of seven tetra-atomic inorganic oxides and six five- and six-atom hydrogenated inorganic oxides are able to predict the anharmonic frequencies compared to explicit anharmonic computations of molecules in the set within an average of 2.2 cm^{-1} and those of molecules from the recent literature within 3.0 cm^{-1}. The prediction of the well-defined M−H stretching frequencies in the associated five- and six-atom hydrides is nearly as successful when the Mg−H containing structures are removed. Even when performance breaks down in the other modes, the scaling factors still give results with errors of the same magnitude as the F12-TZ QFF methodology, making their utilization similarly accurate as explicit QFFs at this level of theory.

Hence, the much more time-consuming QFF portion of the present method may not be necessary to achieve reasonable accuracy on related systems provided that F12-TZ harmonic frequencies are accessible. This would allow for the computation of the anharmonic frequencies of much larger molecules, such as clusters of inorganic oxides containing 20 or more atoms approximating nanoclusters, which would be impossible with the full F12-TZ QFF method. Furthermore, the possibility exists that the addition of more molecules to the training set could improve the heuristic scaling factors for these larger systems, but most are likely well-defined with those determined here because these frequencies are already low and minimally anharmonic. Faster prediction of experimental spectra will help laboratory spectroscopists and astronomers assign molecular carriers to observed and unexplained peaks from various astrophysical infrared sources. Although the quantum chemical prediction of rotational constants still requires more accurate methods at this point than even F12-TZ QFFs, the infrared spectral data can take advantage of the anharmonic scaling factors, pairing well with the infrared capabilities of the upcoming *James Webb Space Telescope*.

Finally, the present work has provided accurate descriptions for the vibrational frequencies and spectroscopic constants of the following inorganic oxides and hyrogenated oxides: $(MgO)_2$, $(AlO)_2$, $(SiO)_2$, $(PO)_2$, $(SO)_2$, $(CaO)_2$, $(TiO)_2$, $HAlMgO_2$, $HMgAlO_2$, $HSiAlO_2$, $HAlSiO_2$, $HAlSiO_3$, and $HSiMgO_2H$. Comparison to existing spectral data shows that the F12-TZ data are, in most cases, fortuitously more accurate than the same level of theory including core electron correlation in-line with previous work.[46,47] The hydride bend has a flat potential, but the stretch is more well-defined. In either case, the M−O bonds are more important for descriptions of the bonding and vibrational structure of these inorganic oxides.

ASSOCIATED CONTENT

Supporting Information

The Supporting Information is available free of charge at https://pubs.acs.org/doi/10.1021/acs.jpca.0c01609.

Force constants, Fermi resonances, and Coriolis resonances (PDF)

AUTHOR INFORMATION

Corresponding Author

Ryan C. Fortenberry − *Department of Chemistry & Biochemistry, University of Mississippi, University, Mississippi 38677-1848, United States;* orcid.org/0000-0003-4716-8225; Email: r410@olemiss.edu

Author

Brent R. Westbrook − *Department of Chemistry & Biochemistry, University of Mississippi, University, Mississippi 38677-1848, United States*

Complete contact information is available at: https://pubs.acs.org/10.1021/acs.jpca.0c01609

Notes

The authors declare no competing financial interest.

ACKNOWLEDGMENTS

This work is supported by NASA grant NNX17AH15G and the NSF grant OIA-1757220. The table of contents graphic background image is courtesy of NASA.

REFERENCES

(1) Savage, B. D.; Sembach, K. R. Interstellar Abundances from Absorption-Line Observations with the Hubble Space Telescope. *Annu. Rev. Astron. Astrophys.* **1996**, *34*, 279−329.

(2) Wenk, H.-R.; Bulakh, A. *Minerals: Their Constitution and Origin*, 1st ed.; Cambridge University Press: Cambridge, U.K., 2004.
(3) Valencia, E. M.; Worth, C. J.; Fortenberry, R. C. Enstatite ($MgSiO_3$) and Forsterite (Mg_2SiO_4) Monomers and Dimers: Highly-Detectable Infrared and Radioastronomical Molecular Building Blocks. *Mon. Not. R. Astron. Soc.* **2020**, *492*, 276−282.
(4) Fortenberry, R. C. The Case for Gas-Phase Astrochemistry without Carbon. *Mol. Astrophys.* **2020**, *18*, 100062.
(5) Jäger, C.; Molster, F.; Dorschner, J.; Henning, T.; Mutschke, H.; Waters, L. Steps toward interstellar silicate mineralogy. IV. The crystalline revolution. *Astron. Astrophys.* **1998**, *339*, 904−916.
(6) Gail, H.-P.; Sedlmayr, E. Mineral Formation in Stellar Winds I. Condensation Sequence of Silicate and Iron Grains in Stationary Oxygen Rich Outflows. *Astron. Astrophys.* **1999**, *347*, 594−616.
(7) Kimura, Y.; Nuth, J. A., III A Seed of Solar Forsterite and Possible New Evolutional Scenario of Cosmic Silicates. *Astrophys. J.* **2009**, *697*, L10−L13.
(8) Speck, A. K.; Whittington, A. G.; Hofmeister, A. M. Disordered Silicates in Space: A Study of Laboratory Spectra of "Amorphous" Silicates. *Astrophys. J.* **2011**, *740*, 93.
(9) Karki, B. B. First-Principles Computation of Mantle Materials in Crystalline and Amorphous Phases. *Phys. Earth Planet. Inter.* **2015**, *240*, 43−69.
(10) Mauney, C. M.; Lazzati, D. The Formation of Astrophysical Mg-Rich Silicate Dust. *Mol. Astrophys.* **2018**, *12*, 1−9.
(11) Zamirri, L.; Macià Escatllar, A.; Mariñoso Guiu, J.; Ugliengo, P.; Bromley, S. T. What Can Infrared Spectra Tell Us about the Crystallinity of Nanosized Interstellar Silicate Dust Grains? *ACS Earth Space Chem.* **2019**, *3*, 2323−2338.
(12) Molster, F. J.; Lim, T. L.; Sylvester, R. J.; Waters, L. B. F. M.; Barlow, M. J.; Beintema, D. A.; Cohen, M.; Cox, P.; Schmitt, B. The Complete ISO Spectrum of NGC 6302. *Astron. Astrophys.* **2001**, *372*, 165−172.
(13) Poteet, C. A.; Megeath, S. T.; Watson, D. M.; Calvet, N.; Remming, I. S.; McClure, M. K.; Sargent, B. A.; Fischer, W. J.; Furlan, E.; Allen, L. E.; et al. A Spitzer Spectrograph Detection of Crystalline Silicates in a Protostellar Envelope. *Astrophys. J., Lett.* **2011**, *733*, L32.
(14) de Vries, B. L.; Acke, B.; Blommaert, J. A. D. L.; Waelkens, C.; Waters, L. B. F. M.; Vandenbussche, B.; Min, M.; Olofsson, G.; Dominik, C.; Decin, L.; et al. Comet-Like Mineralogy of Olivine Crystals in an Extrasolar Proto-Kuiper Belt. *Nature* **2012**, *490*, 74−76.
(15) Gobrecht, D.; Cherchneff, I.; Sarangi, A.; Plane, J. M. C.; Bromley, S. T. Dust Formation in the Oxygen-Rich AGB Star IK Tauri. *Astron. Astrophys.* **2016**, *585*, A6.
(16) Komatsu, M.; Fagan, T. J.; Krot, A. N.; Nagashima, K.; Petaev, M. I.; Kimura, M.; Yamaguchi, A. First Evidence for Silica Condensation within the Solar Protoplanetary Disk. *Proc. Natl. Acad. Sci. U.S.A.* **2018**, *115*, 7497−7502.
(17) Cherchneff, I.; Dwek, E. The Chemistry of Population III Supernova Ejecta. II. The Nucleation of Molecular Clusters as a Diagnostic for Dust in the Early Universe. *Astrophys. J.* **2010**, *713*, 1−24.
(18) Tenenbaum, E. D.; Ziurys, L. M. Millimeter Detection of AlO (X 2Σ+): Metal Oxide Chemistry in the Envelope of VY Canis Majoris. *Astrophys. J.* **2009**, *694*, L59−L63.
(19) Wilson, R. W.; Penzias, A. A.; Jefferts, K. B.; Kutner, M.; Thaddeus, P. Discovery of Interstellar Silicon Monoxide. *Astrophys. J.* **1971**, *167*, L97−L100.
(20) Dickinson, D. F. Detection of Silicon Monoxide at 87 GHz. *Astrophys. J.* **1972**, *175*, L43−L46.
(21) Tenenbaum, E. D.; Woolf, N. J.; Ziurys, L. M. Identification of Phosphorus Monoxide (X 2Πr) in VY Canis Majoris: Detection of the First P−O Bond in Space. *Astrophys. J.* **2007**, *666*, L29−L32.
(22) Gottlieb, C. A.; Ball, J. A. Interstellar Sulfur Monoxide. *Astrophys. J.* **1973**, *184*, L59−L64.
(23) Kamiński, T.; Gottlieb, C. A.; Menten, K. M.; Patel, N. A.; Young, K. H.; Brünken, S.; Müller, H. S. P.; McCarthy, M. C.; Winters, J. M.; Decin, L. Pure Rotational Spectra of TiO and TiO_2 in VY Canis Majoris. *Astron. Astrophys.* **2013**, *551*, A113.
(24) Snyder, L. E.; Hollis, J. M.; Ulich, B. L.; Lovas, F. J.; Johnson, D. R.; Buhl, D. Radio Detection of Interstellar Sulfur Dioxide. *Astrophys. J.* **1975**, *198*, L81−L84.
(25) Turner, B. E. Detection of Interstellar SO^+: A Diagnostic of Dissociative Shock Chemistry. *Astrophys. J.* **1992**, *396*, L107−L110.
(26) Kloska, K. A.; Fortenberry, R. C. Gas-Phase Spectra of MgO Molecules: A Possible Connection from Gas-Phase Molecules to Planet Formation. *Mon. Not. R. Astron. Soc.* **2018**, *474*, 2055−2063.
(27) Bencivenni, L.; Pelino, M.; Ramondo, F. Ab Initio Study on the Al_2O, Al_2O_2, Si_2O_2 and $AlSiO_2$ Oxides and on the $LiAlO_2$ and $NaAlO_2$ Molecules. *J. Mol. Struct.* **1992**, *253*, 109−120.
(28) Xu, G.-L.; Liu, X.-F.; Xie, H.-X.; Zhang, X.-Z.; Liu, Y.-F. Si_2O_2 Molecule: Structure of Ground State and the Excited Properties under Different External Electric Fields. *Chin. Phys. B* **2010**, *19*, 113101.
(29) Desai, S. R.; Wu, H.; Rohlfing, C. M.; Wang, L.-S. A Study of the Structure and Bonding of Small Aluminum Oxide Clusters by Photoelectron Spectroscopy: AlxOy−(x=1-2, y=1-5). *J. Chem. Phys.* **1997**, *106*, 1309.
(30) Khanna, R. K.; Stranz, D. D.; Donn, B. A Spectroscopic Study of Intermediates in the Condensation of Refractory Smokes: Matrix Isolation Experiments of SiO. *J. Chem. Phys.* **1981**, *74*, 2108.
(31) Anderson, J. S.; Ogden, J. S. Matrix Isolation Studies of Group-IV Oxides. I. Infrared Spectra and Structures of SiO, Si_2O_2, and Si_3O_3. *J. Chem. Phys.* **1969**, *51*, 4189.
(32) Schnöckel, H.; Mehner, T.; Plitt, H. S.; Schunck, S. Structure of silicon monoxide dimer: a comparison between aluminum monofluoride dimer, silicon monoxide dimer, and phosphorus mononitride dimer. Matrix infrared investigation and ab initio calculation. *J. Am. Chem. Soc.* **1989**, *111*, 4578−4582.
(33) Huang, X.; Lee, T. J. A Procedure for Computing Accurate Ab Initio Quartic Force Fields: Application to HO_2^+ and H_2O. *J. Chem. Phys.* **2008**, *129*, 044312.
(34) Huang, X.; Lee, T. J. Accurate Ab Initio Quartic Force Fields for NH2−and CCH− and Rovibrational Spectroscopic Constants for Their Isotopologs. *J. Chem. Phys.* **2009**, *131*, 104301.
(35) Huang, X.; Taylor, P. R.; Lee, T. J. Highly Accurate Quartic Force Field, Vibrational Frequencies, and Spectroscopic Constants for Cyclic and Linear C3H3+. *J. Phys. Chem. A* **2011**, *115*, 5005−5016.
(36) Fortenberry, R. C.; Huang, X.; Francisco, J. S.; Crawford, T. D.; Lee, T. J. Quartic Force Field Predictions of the Fundamental Vibrational Frequencies and Spectroscopic Constants of the Cations $HOCO^+$ and $DOCO^+$. *J. Chem. Phys.* **2012**, *136*, 234309.
(37) Huang, X.; Fortenberry, R. C.; Lee, T. J. Spectroscopic Constants and Vibrational Frequencies for l-C_3H^+ and Isotopologues from Highly-Accurate Quartic Force Fields: The Detection of l-C_3H^+ in the Horsehead Nebula PDR Questioned. *Astrophys. J., Lett.* **2013**, *768*, L25.
(38) Zhao, D.; Doney, K. D.; Linnartz, H. Laboratory Gas-Phase Detection of the Cyclopropenyl Cation (c-C3H3+). *Astrophys. J., Lett.* **2014**, *791*, L28.
(39) Fortenberry, R. C.; Huang, X.; Schwenke, D. W.; Lee, T. J. Limited Rotational and Rovibrational Line Lists Computed with Highly Accurate Quartic Force Fields and Ab Initio Dipole Surfaces. *Spectrochim. Acta, Part A* **2014**, *119*, 76−83.
(40) Fortenberry, R. C.; Lee, T. J.; Müller, H. S. P. Excited Vibrational Level Rotational Constants for SiC_2: A Sensitive Molecular Diagnostic for Astrophysical Conditions. *Molec. Astrophys.* **2015**, *1*, 13−19.
(41) Kitchens, M. J. R.; Fortenberry, R. C. The Rovibrational Nature of Closed-Shell Third-Row Triatomics: HOX and HXO, X = Si^+, P, S^+, and Cl. *Chem. Phys.* **2016**, *472*, 119−127.
(42) Fortenberry, R. C. Rovibrational Characterization of the Proton-Bound, Noble Gas Complexes: $ArHNe^+$, $ArHAr^+$, and $NeHNe^+$. *ACS Earth Space Chem.* **2017**, *1*, 60−69.
(43) Bizzocchi, L.; Lattanzi, V.; Laas, J.; Spezzano, S.; Giuliano, B. M.; Prudenzano, D.; Endres, C.; Sipilä, O.; Caselli, P. Accurate Sub-Millimetre Rest Frequencies for $HOCO^+$ and $DOCO^+$ Ions. *Astron. Astrophys.* **2017**, *602*, A34.

https://dx.doi.org/10.1021/acs.jpca.0c01609
J. Phys. Chem. A 2020, 124, 3191−3204

(44) Huang, X.; Valeev, E. F.; Lee, T. J. Comparison of One-Particle Basis Set Extrapolation to Explicitly Correlated Methods for the Calculation of Accurate Quartic Force Fields, Vibrational Frequencies, and Spectroscopic Constants: Application to H_2O, N_2H^+, NO2+, and C_2H_2. *J. Chem. Phys.* **2010**, *133*, 244108.
(45) Agbaglo, D.; Lee, T. J.; Thackston, R.; Fortenberry, R. C. A Small Molecule with PAH Vibrational Properties and a Detectable Rotational Spectrum: c-(C)C3H2, Cyclopropenylidenyl Carbene. *Astrophys. J.* **2019**, *871*, 236.
(46) Agbaglo, D.; Fortenberry, R. C. The Performance of CCSD(T)-F12/aug-cc-pVTZ for the Computation of Anharmonic Fundamental Vibrational Frequencies. *Int. J. Quantum Chem.* **2019**, *119*, No. e25899.
(47) Agbaglo, D.; Fortenberry, R. C. The Performance of Explicitly Correlated Wavefunctions (CCSD(T)-F12b) in the Computation of Anharmonic Vibrational Frequencies. *Chem. Phys. Lett.* **2019**, *734*, 136720.
(48) Pople, J. A.; Schlegel, H. B.; Krishnan, R.; DeFrees, D. J.; Binkley, J. S.; Frisch, M. J.; Whiteside, R. A. Molecular Orbital Studies of Vibrational Frequencies. *Int. J. Quantum Chem.* **1981**, *20*, 269−278.
(49) Hout, R. F.; Hout, J.; Levi, B. A.; Hehre, W. J. Effect of Electron Correlation on Theoretical Vibrational Frequencies. *J. Comput. Chem.* **1982**, *3*, 234−250.
(50) DeFrees, D. J.; McLean, A. D. Molecular Orbital Predictions of the Vibrational Frequencies of Some Molecular Ions. *J. Chem. Phys.* **1985**, *82*, 333−341.
(51) Grev, R. S.; Janssen, C. L.; Schaefer, H. F. Concerning Zeropoint Vibrational Energy Corrections to Electronic Energies. *J. Chem. Phys.* **1991**, *95*, 5128.
(52) Healy, E. F.; Holder, A. An Evaluation of AM1 Calculated Vibrational Frequencies. *J. Mol. Struct.* **1993**, *281*, 141−156.
(53) Pople, J. A.; Scott, A. P.; Wong, M. W.; Radom, L. Scaling Factors for Obtaining Fundamental Vibrational Frequencies and Zero-Point Energies from HF/6-31G* and MP2/6-31G* Harmonic Frequencies. *Isr. J. Chem.* **1993**, *33*, 345−350.
(54) Rauhut, G.; Pulay, P. Transferable Scaling Factors for Density Functional Derived Vibrational Force Fields. *J. Phys. Chem.* **1995**, *99*, 3093−3100.
(55) Scott, A. P.; Radom, L. Harmonic Vibrational Frequencies: An Evaluation of Hartree-Fock, Møller-Plesset, Quadratic Configuration Interaction, Density Functional Theory, and Semiempirical Scale Factors. *J. Phys. Chem.* **1996**, *100*, 16502−16513.
(56) Wong, M. W. Vibrational Frequency Prediction Using Density Functional Theory. *Chem. Phys. Lett.* **1996**, *256*, 391−399.
(57) Fast, P. L.; Corchado, J.; Sanchez, M. L.; Truhlar, D. G. Optimized Parameters for Scaling Correlation Energy. *J. Phys. Chem. A* **1999**, *103*, 3139−3143.
(58) Curtiss, L. A.; Redfern, P. C.; Raghavachari, K.; Pople, J. A. Gaussian-3X (G3X) Theory: Use of Improved Geometries, Zero-Point Energies, and Hartree-Fock Basis Sets. *J. Chem. Phys.* **2001**, *114*, 108−117.
(59) Halls, M. D.; Velkovski, J.; Schlegel, H. B. Harmonic Frequency Scaling Factors for Hartree-Fock, S-VWN, B-LYP, B3-LYP, B3-PW91 and MP2 with the Sadlej pVTZ Electric Property Basis Set. *Theor. Chem. Acc.* **2001**, *105*, 413−421.
(60) Lynch, B. J.; Truhlar, D. G. How Well Can Hybrid Density Functional Methods Predict Transition State Geometries and Barrier Heights? *J. Phys. Chem. A* **2001**, *105*, 2936−2941.
(61) Sinha, P.; Boesch, S. E.; Gu, C.; Wheeler, R. A.; Wilson, A. K. Harmonic Vibrational Frequencies: Scaling Factors for HF, B3LYP, and MP2 Methods in Combination with Correlation Consistent Basis Sets. *J. Phys. Chem. A* **2004**, *108*, 9213−9217.
(62) Zhao, Y.; Lynch, B. J.; Truhlar, D. G. Doubly Hybrid Meta DFT: New Multi-Coefficient Correlation and Density Functional Methods for Thermochemistry and Thermochemical Kinetics. *J. Phys. Chem. A* **2004**, *108*, 4786−4791.
(63) Zhao, Y.; Lynch, B. J.; Truhlar, D. G. Development and Assessment of a New Hybrid Density Functional Model for Thermochemical Kinetics. *J. Phys. Chem. A* **2004**, *108*, 2715−2719.
(64) Zhao, Y.; Truhlar, D. G. Hybrid Meta Density Functional Theory Methods for Thermochemistry, Thermochemical Kinetics, and Noncovalent Interactions: The MPW1B95 and MPWB1K Models and Comparative Assessments for Hydrogen Bonding and van der Waals Interactions. *J. Phys. Chem. A* **2004**, *108*, 6908−6918.
(65) Andersson, M. P.; Uvdal, P. New Scale Factors for Harmonic Vibrational Frequencies Using the B3LYP Density Functional Method with the Triple-ζ Basis Set 6-311+G(d,p). *J. Phys. Chem. A* **2005**, *109*, 2937−2941.
(66) Csonka, G. I.; Ruzsinszky, A.; Perdew, J. P. Estimation, Computation, and Experimental Correction of Molecular Zero-Point Vibrational Energies. *J. Phys. Chem. A* **2005**, *109*, 6779−6789.
(67) Schultz, N. E.; Zhao, Y.; Truhlar, D. G. Databases for Transition Element Bonding: Metal-Metal Bond Energies and Bond Lengths and Their Use To Test Hybrid, Hybrid Meta, and Meta Density Functionals and Generalized Gradient Approximations. *J. Phys. Chem. A* **2005**, *109*, 4388−4403.
(68) Tantirungrotechai, Y.; Phanasant, K.; Roddecha, S.; Surawatanawong, P.; Sutthikhum, V.; Limtrakul, J. Scaling Factors for Vibrational Frequencies and Zero-Point Vibrational Energies of Some Recently Developed Exchange-Correlation Functionals. *J. Mol. Struct.* **2006**, *760*, 189−192.
(69) Merrick, J. P.; Moran, D.; Radom, L. An Evaluation of Harmonic Vibrational Frequency Scale Factors. *J. Phys. Chem. A* **2007**, *111*, 11683−11700.
(70) Werner, H.-J.; Knowles, P. J.; Knizia, G.; Manby, F. R.; Schütz, M.; Celani, P.; Györffy, W.; Kats, D.; Korona, T.; Lindh, R. et al. *MOLPRO*, version 2015.1, a Package of ab Initio Programs, 2015; see http://www.molpro.net.
(71) Raghavachari, K.; Trucks, G. W.; Pople, J. A.; Replogle, E. Highly Correlated Systems: Structure, Binding Energy and Harmonic Vibrational Frequencies of Ozone. *Chem. Phys. Lett.* **1989**, *158*, 207−212.
(72) Adler, T. B.; Knizia, G.; Werner, H.-J. A Simple and Efficient CCSD(T)-F12 Approximation. *J. Chem. Phys.* **2007**, *127*, 221106.
(73) Knizia, G.; Adler, T. B.; Werner, H.-J. Simplified CCSD(T)-F12 Methods: Theory and Benchmarks. *J. Chem. Phys.* **2009**, *130*, 054104.
(74) Peterson, K. A.; Adler, T. B.; Werner, H.-J. Systematically Convergent Basis Sets for Explicitly Correlated Wavefunctions: The Atoms H, He, B-Ne, and Al-Ar. *J. Chem. Phys.* **2008**, *128*, 084102.
(75) Hill, J. G.; Peterson, K. A. Correlation Consistent Basis Sets for Explicitly Correlated Wavefunctions: Valence and Core-Valence Basis Sets for Li, Be, Na, and Mg. *Phys. Chem. Chem. Phys.* **2010**, *12*, 10460−10468.
(76) Koput, J.; Peterson, K. A. Ab Initio Potential Energy Surface and Vibrational-Rotational Energy Levels of $X^2\Sigma^+$CaOH. *J. Phys. Chem. A* **2002**, *106*, 9595−9599.
(77) Balabanov, N. B.; Peterson, K. A. Systematically Convergent Basis Sets for Transition Metals. I. All-Electron Correlation Consistent Basis Sets for the 3d Elements Sc-Zn. *J. Chem. Phys.* **2005**, *123*, 064107.
(78) Weigend, F.; Ahlrichs, R. Balanced Basis Sets of Split Valence, Triple Zeta Valence and Quadruple Zeta Valence Quality for H to Rn: Design and Assessment of Accuracy. *Phys. Chem. Chem. Phys.* **2005**, *7*, 3297.
(79) Radoń, M. Benchmarking Quantum Chemistry Methods for Spin-State Energetics of Iron Complexes against Quantitative Experimental Data. *Phys. Chem. Chem. Phys.* **2019**, *21*, 4854.
(80) Frisch, M. J.; Trucks, G. W.; Schlegel, H. B.; Scuseria, G. E.; Robb, M. A.; Cheeseman, J. R.; Scalmani, G.; Barone, V.; Petersson, G. A.; Nakatsuji, H. et al. *Gaussian 16*, Revision C.01; Gaussian Inc: Wallingford CT, 2016.
(81) Møller, C.; Plesset, M. S. Note on an Approximation Treatment for Many-Electron Systems. *Phys. Rev.* **1934**, *46*, 618−622.
(82) Becke, A. D. Density-Functional Thermochemistry. III. The Role of Exact Exchange. *J. Chem. Phys.* **1993**, *98*, 5648−5652.

https://dx.doi.org/10.1021/acs.jpca.0c01609
J. Phys. Chem. A 2020, 124, 3191−3204

(83) Yang, W.; Parr, R. G.; Lee, C. Various Functionals for the Kinetic Energy Density of an Atom or Molecule. *Phys. Rev. A: At., Mol., Opt. Phys.* **1986**, *34*, 4586−4590.
(84) Lee, C.; Yang, W.; Parr, R. G. Development of the Colle-Salvetti Correlation-Energy Formula into a Functional of the Electron Density. *Phys. Rev. B: Condens. Matter Mater. Phys.* **1988**, *37*, 785−789.
(85) Yu, Q.; Bowman, J. M.; Fortenberry, R. C.; Mancini, J. S.; Lee, T. J.; Crawford, T. D.; Klemperer, W.; Francisco, J. S. The Structure, Anharmonic Vibrational Frequencies, and Intensities of $NNHNN^+$. *J. Phys. Chem. A* **2015**, *119*, 11623−11631.
(86) Finney, B.; Fortenberry, R. C.; Francisco, J. S.; Peterson, K. A. A Spectroscopic Case for SPSi Detection: The Third-Row in a Single Molecule. *J. Chem. Phys.* **2016**, *145*, 124311.
(87) Fortenberry, R. C.; Lee, T. J. Computational Vibrational Spectroscopy for the Detection of Molecules in Space. *Annu. Rep. Comput. Chem.* **2019**, *15*, 173−202.
(88) Hill, J. G.; Mazumder, S.; Peterson, K. A. Correlation Consistent Basis Sets for Molecular Core-Valence Effects with Explicitly Correlated Wave Functions: The Atoms B-Ne and Al-Ar. *J. Chem. Phys.* **2010**, *132*, 054108.
(89) Allen and co-workers, 2005; INTDER 2005 is a general program written by Allen and co-workers, which performs vibrational analysis and higher-order non-linear transformations.
(90) Mills, I. M. In *Molecular Spectroscopy—Modern Research*; Rao, K. N., Mathews, C. W., Eds.; Academic Press: New York, 1972; pp 115−140.
(91) Watson, J. K. G. In *Vibrational Spectra and Structure*; Durig, J. R., Ed.; Elsevier: Amsterdam, 1977; pp 1−89.
(92) Papousek, D.; Aliev, M. R. *Molecular Vibration-Rotation Spectra*; Elsevier: Amsterdam, 1982.
(93) Gaw, J. F.; Willets, A.; Green, W. H.; Handy, N. C. *SPECTRO program*, version 3.0, 1996.
(94) Martin, J. M. L.; Lee, T. J.; Taylor, P. R.; François, J. P. The Anharmonic Force Field of Ethylene, C_2H_4, by Means of Accurate ab Initio Calculations. *J. Chem. Phys.* **1995**, *103*, 2589−2602.
(95) Martin, J. M. L.; Taylor, P. R. Accurate ab Initio Quartic Force Field for trans-HNNH and Treatment of Resonance Polyads. *Spectrochim. Acta, Part A* **1997**, *53*, 1039−1050.
(96) Fortenberry, R. C.; Francisco, J. S. Quartic Force Field-Derived Vibrational Frequencies and Spectroscopic Constants for the Isomeric Pair SNO and OSN and Isotopologues. *J. Chem. Phys.* **2015**, *143*, 084308.
(97) Fortenberry, R. C.; Francisco, J. S. Energetics, Structure, and Rovibrational Spectroscopic Properties of the Sulfurous Anions SNO^- and OSN^-. *J. Chem. Phys.* **2015**, *143*, 184301.
(98) DeVine, J. A.; Babin, M. C.; Neumark, D. M. Photoelectron Spectra of Al2O2−and SAl3O3− vialow Electron Velocity-Map Imaging. *Faraday Discuss.* **2019**, *217*, 235−255.
(99) Andrews, L.; Chertihin, G. V.; Thompson, C. A.; Dillon, J.; Byrne, S.; Bauschlicher, C. W., Jr. Infrared Spectra and Quantum Chemical Calculations of Group 2 MO_2, O_2MO_2, and Related Molecules. *J. Phys. Chem.* **1996**, *100*, 10088−10099.
(100) Lee, T. J.; Taylor, P. R. A Diagnostic for Determining the Quality of Single-Reference Electron Correlation Methods. *Int. J. Quantum Chem.* **1989**, *36*, 199−207.

https://dx.doi.org/10.1021/acs.jpca.0c01609
J. Phys. Chem. A 2020, 124, 3191−3204